

Antiferromagnetic Nuclear Resonance in the Quasi-Two-Dimensional (CuBr)LaNb₂O₇

Makoto YOSHIDA*, Nobuyuki OGATA, Masashi TAKIGAWA†, Taro KITANO¹, Hiroshi KAGEYAMA¹, Yoshitami AJIRO¹, and Kazuyoshi YOSHIMURA¹

Institute for Solid State Physics, University of Tokyo, Kashiwa, Chiba 277-8581

¹*Department of Chemistry, Graduate School of Science, Kyoto University, Kyoto 606-8502*

We report nuclear magnetic resonance (NMR) studies in the antiferromagnetic state of the quasi-two-dimensional (CuBr)LaNb₂O₇. The NMR spectra at zero magnetic field and 4.2 K indicate a unique Cu and Br sites with an internal field of 5.7 T (at Cu) and 16.4 T (at Br), confirming a magnetic order. For the large internal field at the Br sites to be compatible with the collinear antiferromagnetic order observed by neutron diffraction experiments (N. Oba *et al.*, J. Phys. Soc. Jpn. **75**, (2006) 113601), the Br atoms must move significantly off the center of the square of the Cu sublattice so that the Br nuclei couple predominantly to two parallel Cu moments. While invalidating the frustrated J_1 - J_2 model defined on a C_4 -symmetric square lattice, our results are compatible with the structural model proposed for (CuCl)LaNb₂O₇ by Yoshida *et al.* (J. Phys. Soc. Jpn. **76**, (2007) 104703).

KEYWORDS: NMR, (CuBr)LaNb₂O₇, quantum spin system, collinear order, structural distortion

1. Introduction

The recent successful synthesis of a new Dion-Jacobson series of quasi-two-dimensional quantum spin systems (CuX) $A_{n-1}B_nO_{3n+1}$ ($A = \text{La}^{3+}, \text{Ca}^{2+}, \text{Na}^+, \dots$, $B = \text{Nb}^{5+}, \text{Ta}^{5+}, \text{Ti}^{4+}$, $X = \text{Cl}, \text{Br}$, $n = 2, 3, 4, \dots$) by ion-exchange reaction has enabled us to explore a wide variety of novel quantum phenomena in a common structure of the CuX magnetic layers, where Cu²⁺ ions (spin 1/2) form a square lattice with X⁻ ions located at the center of the square.¹⁻⁷ For example, (CuCl)LaNb₂O₇ has a singlet ground state with an excitation gap of 2.3 meV² and shows an intriguing phase transition in magnetic fields.^{3,6,7} On the other hand, a collinear antiferromagnetic order at the wave vector $\mathbf{Q} = (\pi, 0, \pi)$ occurs below $T_N = 32$ K in (CuBr)LaNb₂O₇.⁴ Furthermore, (CuBr)Sr₂Nb₃O₁₀ with a wider interlayer separation exhibits a puzzling magnetization plateau at 1/3 of the saturation.⁵

Early structural studies on (CuX)LaNb₂O₇ ($X = \text{Cl}$ or Br) reported the tetragonal $P4/mmm$ space group, where both the Cu and the X sites have the C_4 symmetry^{1,8} (Fig. 1). Based on this, a Heisenberg spin model with the nearest neighbor exchange J_1 and the second nearest neighbor exchange J_2 (the so-called J_1 - J_2 model) was considered an appropriate model. In fact, extensive theoretical work on the frustrated J_1 - J_2 model predicts a collinear antiferromagnetic order with the wave vector $(\pi, 0)$ for $J_2 \gg |J_1|$ and a spin-singlet phase in the highly frustrated region $J_2/|J_1| \sim 0.5$ both for the positive (antiferromagnetic)^{9,10} and the negative (ferromagnetic)¹¹ values of J_1 . This appears to be corroborated nicely by the experimental observation of the collinear order in (CuBr)LaNb₂O₇ and the singlet ground state in (CuCl)LaNb₂O₇. The analysis of the susceptibility and the magnetization process indicated that J_1 is ferromag-

netic in (CuX)LaNb₂O₇.

However, structural information obtained from subsequent experiments has raised serious doubt against the validity of the J_1 - J_2 model. The neutron diffraction experiments on (CuCl)LaNb₂O₇¹² suggested significant deviation of the Cl position from the center of the Cu square along the [100] direction. The Synchrotron X-ray diffraction on (FeCl)LaNb₂O₇¹³ and the transmission electron microscopy (TEM) measurements on (CuCl)LaNb₂O₇⁷ revealed a superlattice reflections indicating an enlarged $2a \times 2b \times c$ unit cell. The nuclear magnetic resonance (NMR) and the nuclear quadrupole resonance (NQR) experiments in (CuCl)LaNb₂O₇⁷ demonstrated absence of the four-fold symmetry around the c -axis at both the Cu and the Cl sites. In particular, the

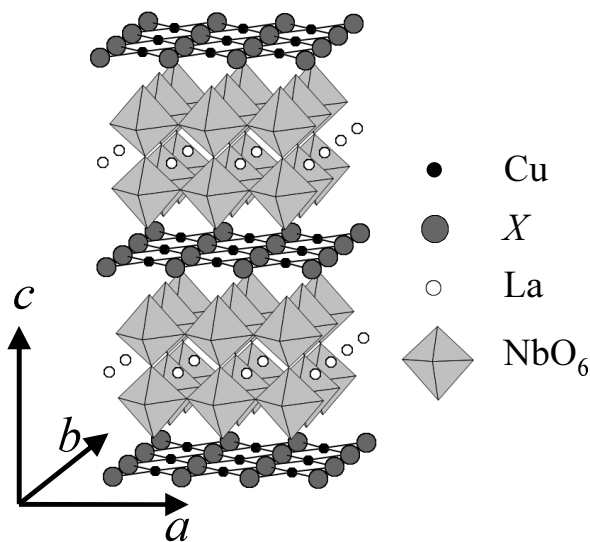


Fig. 1. Schematic crystal structure of (CuX)LaNb₂O₇ ($X = \text{Cl}, \text{Br}$).¹

*E-mail address: yopida@issp.u-tokyo.ac.jp

†E-mail address: masashi@issp.u-tokyo.ac.jp

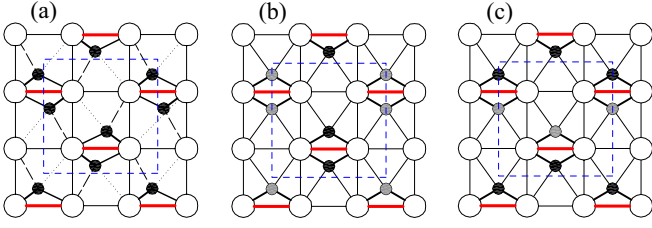


Fig. 2. (color online). Possible structures of the CuCl plane proposed for $(\text{CuCl})\text{LaNb}_2\text{O}_7$.⁷⁾ The open and solid circles represent the Cu and Cl atoms, respectively. In (a), The Cl atoms moves from the ideal $(0, 0, 1/2)$ position to $(x, y, 1/2)$, $(-x, y, 1/2)$, $(x, -y, 1/2)$, or $(-x, -y, 1/2)$ and are still on the same plane as the Cu atoms. In (b) and (c), a half of the Cl atoms moves up to $(x, 0, 1/2 + \delta)$ or $(-x, 0, 1/2 + \delta)$ (black circles) and another half moves down to $(x, 0, 1/2 - \delta)$ or $(-x, 0, 1/2 - \delta)$ (grey circles). The enlarged unit cell is shown by the blue dashed lines. Note that both Cu and Cl occupy a unique crystallographic sites for all cases. The singlet dimer bonds are shown by the thick red lines.

principal axis of the electric field gradient (EFG) tensor at the Cu sites with the largest principal value was found to be perpendicular to the c -axis, providing conclusive evidence for a drastic change of the local structure from the tetragonal $P4/mmm$ symmetry. Yet observation of a single sharp NQR line for the Cu and the Cl nuclei guarantees that they both occupy a unique crystallographic site without significant disorder. Yoshida *et al.* has proposed possible structural models of the CuCl planes in $(\text{CuCl})\text{LaNb}_2\text{O}_7$, which are compatible with the NMR, NQR, and TEM results⁷⁾ (Fig. 2). In these models with orthorhombic distortion, displacement of Cl atoms generates different exchange couplings among the nearest neighbor Cu bonds, which were originally equivalent in the undistorted structure. The models shown in Fig. 2 where the strongest antiferromagnetic bonds are shown by the red (thick) lines then naturally lead to a dimer singlet ground state.

To obtain further insight into the structure and the magnetism in $(\text{CuX})\text{LaNb}_2\text{O}_7$, we performed the NMR experiments in the collinear ordered phase of $(\text{CuBr})\text{LaNb}_2\text{O}_7$. The internal field from ordered magnetic moments and the EFG at the nuclear sites provide useful information on the local structure. We found a unique large internal field at both the Cu and the Br sites at 4.2 K, conforming a magnetic order. However, if the Br nuclei coupled equally to the four neighboring Cu spins, the internal fields from these spins would have to be cancelled out to yield zero net field for the collinear AF structure. Thus our results provide conclusive evidence for lower symmetry of the Br sites that allows the Br nuclei to couple dominantly to only two parallel Cu spins.

2. Experimental Results

The powder sample of $(\text{CuBr})\text{LaNb}_2\text{O}_7$ was synthesized by the following ion-exchange reaction as described in Refs. 2 and 4,



NMR spectra were obtained by recording the integrated intensity of the spin-echo signal at discrete frequencies. NMR spin-echo signal was observed at zero magnetic field and the temperature of 4.2 K in the frequency range 30-260 MHz.

The obtained spectra are shown in Figs. 3(a) and 3(b) for the frequency ranges 80-260 MHz and 30-100 MHz, respectively. As shown in Fig. 3(a), sharp six resonance lines are observed in the frequency range 100-260 MHz, which can be grouped into three pairs. The peak frequencies are determined by fitting each line to a Lorentzian and the results are shown in Table I. A natural interpretation for such a spectrum is the superposition of resonance from two kinds of spin 3/2 nuclei, both having the dominant magnetic Zeeman interaction split by the subdominant electric quadrupole interaction. On the other hand, rather broad lines with only five visible peaks are observed in the frequency range 30-100 MHz, as shown in Fig. 3(b). However, we have succeeded in decomposing the observed spectrum into three pairs of Lorentzian as shown by the red dashed lines. Thus the spectrum below 100 MHz can be interpreted again by two types of spin 3/2 nuclei with dominant magnetic Zeeman interaction and subdominant quadrupole interaction. The peak frequencies in this frequency range are also listed in Table I. There are indeed four spin 3/2 nuclear species contained in $(\text{CuBr})\text{LaNb}_2\text{O}_7$, which are ^{63}Cu , ^{65}Cu , ^{79}Br , and ^{81}Br . The values of their nuclear gyromagnetic ratio ($^\alpha\gamma$) and the isotopic ratios of the nuclear magnetic moments and the nuclear quadrupole moments ($^\alpha Q$) are listed in Table II, where α stands for the mass number.

3. Analysis I

We first assign the resonance lines in Fig. 3(a)(b) to the four nuclear species. The NMR resonance frequencies for a spin I nucleus in zero magnetic field is generally determined by the following Hamiltonian,^{14,15)}

$$\begin{aligned} \mathcal{H} &= \mathcal{H}_m + \mathcal{H}_q, \\ \mathcal{H}_m &= -h^\alpha\gamma\mathbf{I} \cdot \mathbf{B}_{\text{int}} \\ \mathcal{H}_q &= \frac{h\nu_Q}{6} \left[3I_z^2 - I^2 + \frac{1}{2}\eta(I_+^2 + I_-^2) \right] \end{aligned} \quad (2)$$

with

$$\nu_Q = \frac{3e^\alpha Q}{2I(2I-1)h} V_{zz}, \quad (3)$$

where \mathcal{H}_m (\mathcal{H}_q) describes the magnetic Zeeman (electric quadrupole) interaction, h is the Planck's constant, \mathbf{B}_{int} is the internal (hyperfine) magnetic field at the nuclear sites produced by the electronic magnetic moments, and $V_{zz} = \partial^2 V / \partial z^2$ is the z -component of the electric field gradient (EFG) tensor at the nucleus. Here x , y and z denote the principal axes of the EFG tensor satisfying the relation $|V_{xx}| \leq |V_{yy}| \leq |V_{zz}|$ and the asymmetry parameter of the EFG is defined as $\eta = (V_{xx} - V_{yy}) / V_{zz}$ ($0 \leq \eta \leq 1$, note that $V_{xx} + V_{yy} + V_{zz} = 0$). If the quadrupole interaction is absent, the $2I + 1$ nuclear spin levels are equally split by the Zeeman interaction, giving rise to a single resonance frequency

$$\nu_0 = ^\alpha\gamma B_{\text{int}}. \quad (4)$$

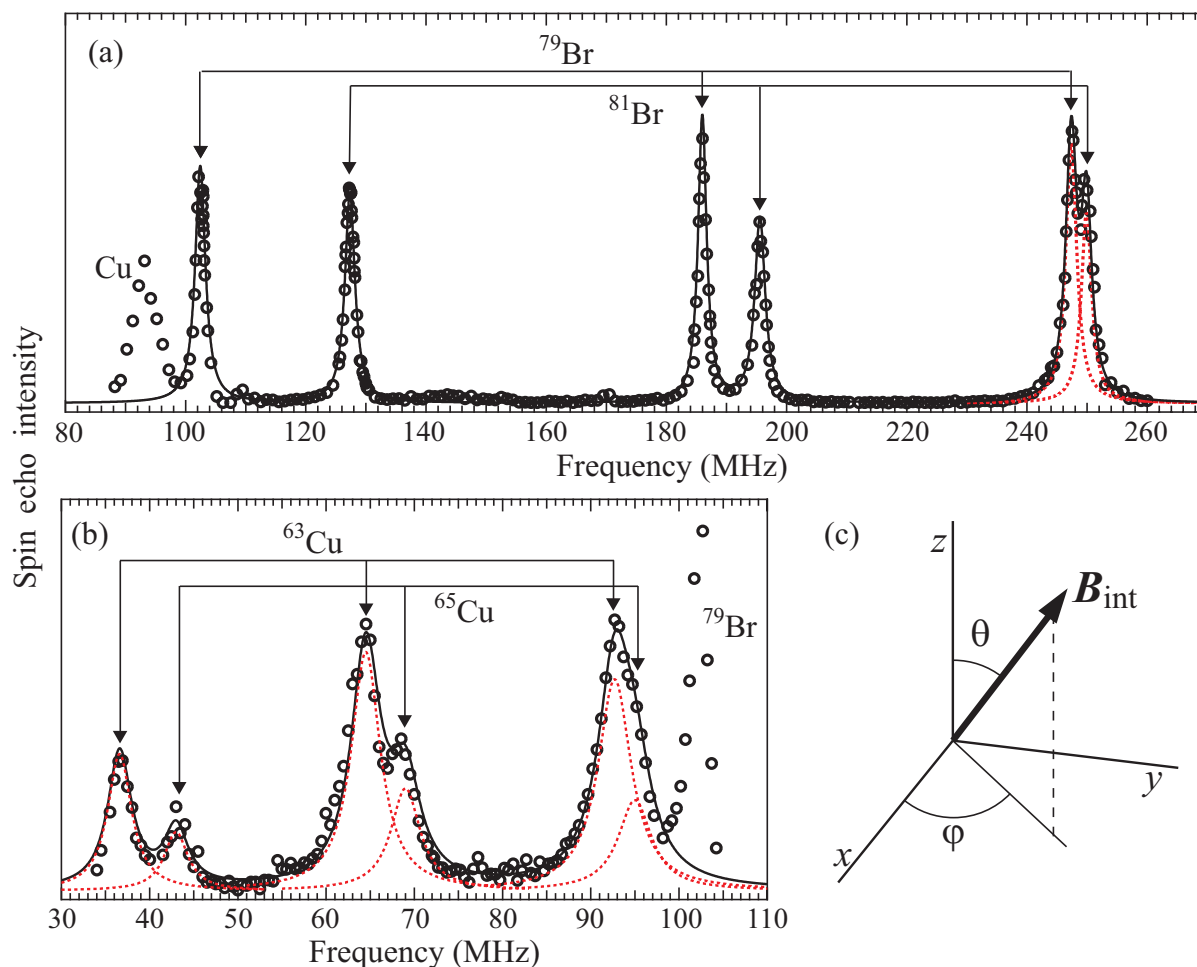


Fig. 3. (color online) The NMR spectra obtained at zero magnetic field and 4.2 K (open circles) for the frequency ranges (a) 80-260 MHz and (b) 30-110 MHz. The black solid lines show the fitting to the sum of six Lorentz functions and the red dashed lines represent the decomposition into each line. (c) Definition of the polar and the azimuthal angles specifying the direction of the internal field with respect to the principal axes of the electric field gradient (EFG).

Table I. Peak frequencies of the NMR spectra in Fig. 3.

	ν_{sl} (MHz)	ν_c (MHz)	ν_{sh} (MHz)
^{63}Cu	36.6 ± 0.3	64.5 ± 0.3	92.7 ± 0.5
^{65}Cu	43.0 ± 0.5	69.0 ± 0.5	95.0 ± 1.0
^{79}Br	102.44 ± 0.1	185.98 ± 0.05	247.36 ± 0.2
^{81}Br	127.34 ± 0.1	195.56 ± 0.1	249.9 ± 0.2

Table II. Values and isotopic ratios of nuclear moments¹⁷⁾

Cu	$^{63}\gamma$ (MHz/T)	$^{65}\gamma$ (MHz)/T	$^{65}\gamma/^{63}\gamma$	$^{65}Q/^{63}Q$
	11.2893	12.0932	1.0712	0.9252
Br	$^{79}\gamma$ (MHz/T)	$^{81}\gamma$ (MHz)/T	$^{81}\gamma/^{79}\gamma$	$^{81}Q/^{79}Q$
	10.6671	11.4984	1.0779	0.8354

A finite value of the quadrupole coupling ν_Q causes the resonance to split into $2I$ lines. The frequencies of the split lines depend on the orientation of the internal magnetic field relative to the principal axes of the EFG. We define the polar and the azimuthal angles θ and ϕ specifying the direction of \mathbf{B}_{int} with respect to the principal axes of the EFG as shown in Fig. 3(c).

When the magnetic Zeeman interaction is dominant

over the quadrupole interaction, $^{\alpha}\gamma\mathbf{B}_{int} \gg \nu_Q$, which indeed turns out to be case for the NMR spectra in Fig. 3, the resonance frequencies can be calculated by the perturbation theory up to second order with reasonably good accuracy. For the case of $I = 3/2$, there are three resonance lines; the central line, the high frequency satellite and the low frequency satellite lines, whose frequencies are denoted by ν_c , ν_{hs} , and ν_{ls} . The perturbation theory gives the following expression,

$$\nu_c = \nu_0 + \delta\nu_c^{(2)} \quad (5a)$$

$$\nu_{hs} = \nu_0 + \delta\nu^{(1)} + \delta\nu_s^{(2)} \quad (5b)$$

$$\nu_{ls} = \nu_0 - \delta\nu^{(1)} + \delta\nu_s^{(2)}. \quad (5c)$$

The first order shift $\delta\nu^{(1)}$ and the second order shifts $\delta\nu_c^{(2)}$ and $\delta\nu_s^{(2)}$ are expressed as¹⁶⁾

$$\delta\nu^{(1)} = (\nu_Q/2) | 3 \cos^2 \theta - 1 + \eta \cos 2\phi \sin^2 \theta | \quad (6a)$$

$$\begin{aligned} \delta\nu_c^{(2)} = & (\nu_Q^2/12\nu_0) \{ -(9/4) \sin^2 \theta (9 \cos^2 \theta - 1) \\ & + (3/2) \eta \cos 2\phi \sin^2 \theta (9 \cos^2 \theta + 1) \\ & + \eta^2 (-2 + 3 \cos^2 \theta + (9/4) \cos^2 2\phi \sin^4 \theta) \} \quad (6b) \end{aligned}$$

$$\delta\nu_s^{(2)} = (\nu_Q^2/12\nu_0) \sin^2 \theta \{18 \cos^2 \theta - 12\eta \cos 2\phi \cos^2 \theta + 2\eta^2(1 - \cos^2 2\phi \sin^2 \theta)\}. \quad (6c)$$

In general, the n -th order shifts $\delta\nu_{c,hs,ls}^{(n)}$ for the three resonance lines satisfy the relations, $\delta\nu_c^{(n)} = 0$ and $\delta\nu_{hs}^{(n)} = -\delta\nu_{ls}^{(n)}$ for odd n and $\delta\nu_{hs}^{(n)} = \delta\nu_{ls}^{(n)}$ for even n .

From Eqs. (3), (5b), (5c) and (6a), one finds that the separation between the two satellite lines is proportional to the nuclear quadrupole moment,

$$\nu_{hs} - \nu_{ls} = 2\delta\nu^{(1)} \propto {}^\alpha Q. \quad (7)$$

This means that the ratio of this separation for the two isotopes on the same chemical and magnetic environment is equal to the ratio of their nuclear quadrupole moments. The NMR spectra in the two panels of Fig. 3 both show two sets of quadrupole split three lines. The ratio of the difference between the highest and the lowest frequencies obtained from the data in Table I is 0.8457 for the spectrum in (a) and 0.9269 for the spectrum in (b). These values are indeed very close to the isotopic ratio of the nuclear quadrupole moments for Br (0.8354) and Cu (0.9251) shown in the Table II, allowing us to assign the resonance lines as indicated in Fig. 3 and Table I. The first order quadrupole shifts are obtained as

$$\delta\nu^{(1)} = 28.1 \text{ (26.0) MHz for } {}^{63}\text{Cu} \text{ (} {}^{65}\text{Cu)} \quad (8a)$$

$$\delta\nu^{(1)} = 72.46 \text{ (61.28) MHz for } {}^{79}\text{Br} \text{ (} {}^{81}\text{Br)}. \quad (8b)$$

These values are much smaller than the Zeeman frequencies, which is approximately equal to the center line frequency shown in Table I. Therefore, our use of the perturbation theory is justified.

If we neglect the second order quadrupole shift, the magnitude of the internal field B_{int} can be crudely estimated from the center line frequency as $B_{\text{int}} \approx 5.7$ T for the Cu sites and $B_{\text{int}} \approx 17$ T for the Br sites. More accurate determination is described in the next section. The existence of such large internal fields at zero magnetic field is the direct evidence for a magnetically ordered state with spontaneous magnetic moments, consistent with the neutron diffraction experiments.⁴⁾

4. Analysis II

In this section, we try to determine the internal field, the EFG, and their relative orientation from the NMR frequencies for both the Br and the Cu sites. The nuclear Hamiltonian Eq. (2) is specified by five parameters, B_{int} , ν_Q , η , θ , and ϕ . Their values are independent of isotopes except for ν_Q , which is proportional to the nuclear quadrupole moment (Eq. 3). Although the second order perturbation expression, Eqs. (5a)-(5c) with Eqs. (6a)-(6c), gives reasonably accurate resonance frequencies, it contains only four independent parameters, ν_0 , $\nu^{(1)}$, $\nu_c^{(2)}$, and $\nu_s^{(2)}$. Therefore, we must examine the higher order terms to determine all the parameters of the Hamiltonian. In what follows, we first use the perturbation expression to find an appropriate range of the parameter values. We then diagonalize the Hamiltonian Eq. (2) numerically to calculate the resonance frequencies exactly and seek the best parameter values which mini-

mizes χ^2 defined as $\chi^2 = \sum_{\alpha,k} [(\alpha\nu_k^{obs} - \alpha\nu_k^{cal})^2 / \alpha\sigma_k^2]$, where $\alpha\nu_k^{obs}$ ($\alpha\nu_k^{cal}$) is the observed (calculated) resonance frequency of the k -th line ($k = c, hs, \text{ or } ls$) for the isotope α and $\alpha\sigma_k$ is the experimental uncertainty listed in Table I.

For the case of Br spectrum showing sharp lines, the frequencies can be determined quite accurately. We found that nearly a unique set of parameters can be obtained already by the perturbation analysis. For the case of Cu showing rather broad spectrum, however, we were not able to determine the parameters completely.

4.1 Br sites

We first determine each term in the perturbation expression from the observed resonance frequencies for the two Br isotopes. From Eqs. (4) and (6a)-(6c), the values of each term in the perturbation expression for the two isotopes can be related as

$${}^{81}\nu_0 = ({}^{81}\gamma/{}^{79}\gamma) {}^{79}\nu_0 = 1.0779 \times {}^{79}\nu_0 \quad (9a)$$

$${}^{81}\delta\nu^{(1)} = ({}^{81}Q/{}^{79}Q) {}^{79}\delta\nu^{(1)} = 0.8354 \times {}^{79}\delta\nu^{(1)} \quad (9b)$$

$${}^{81}\delta\nu_{c,s}^{(2)} = \frac{({}^{81}Q/{}^{79}Q)^2}{({}^{81}\gamma/{}^{79}\gamma)} {}^{79}\delta\nu_{c,s}^{(2)} = 0.6474 \times {}^{79}\delta\nu_{c,s}^{(2)}. \quad (9c)$$

From the observed values of ${}^{79}\nu_c$ and ${}^{81}\nu_c$ (Table I), we obtain ${}^{79}\nu_0$ and ${}^{79}\delta\nu_c^{(2)}$, using Eqs. (5a), (9a) and (9c), ${}^{79}\nu_0 = 174.57 \pm 0.14$ MHz, ${}^{79}\delta\nu_c^{(2)} = 11.41 \pm 0.17$ MHz. (10)

Then from the observed values of ${}^{79}\nu_{ls}$ and ${}^{79}\nu_{hs}$ and Eq. (5b) and (5c), we obtain

$${}^{79}\delta\nu^{(1)} = 72.46 \pm 0.14 \text{ MHz, } {}^{79}\delta\nu_s^{(2)} = 0.33 \pm 0.14 \text{ MHz.} \quad (11)$$

We now use the above results to find the possible range of parameter values in the nuclear Hamiltonian. Note that the second order shift for the satellite lines ${}^{79}\delta\nu_s^{(2)}$ (Eq. 11) is very small compared with that for the central line ${}^{79}\delta\nu_c^{(2)}$ (Eq. 10). This puts strong constraints as we see below. First, by noting that the upper limit of the right-hand-side of Eq. (6a) is set by ν_Q , we obtain ${}^{79}\delta\nu^{(1)} \leq {}^{79}\nu_Q$. The experimental value of ${}^{79}\delta\nu^{(1)}$ in Eq. (11) then sets a lower limit for ${}^{79}\nu_Q$, ${}^{79}\nu_Q \geq 72.46$ MHz. Next, putting this lower limit and the experimental value of ${}^{79}\nu_0$ in Eq. (10) into Eq. (6c), we obtain

$${}^{79}\delta\nu_s^{(2)} \geq 2.506(1-\mu)\{(18-12\eta\alpha+2\eta^2\alpha^2)\mu+2\eta^2(1-\alpha^2)\}, \quad (12)$$

where we defined $\mu = \cos^2 \theta$ and $\alpha = \cos 2\phi$. Note that the minimum of the right-hand-side of Eq. (12) is located at $\eta = 1$ and $\alpha = 1$ within the defined range $0 \leq \eta \leq 1$, $-1 \leq \alpha \leq 1$ for any value of μ . Therefore,

$${}^{79}\delta\nu_s^{(2)} \geq 20.05\mu(1-\mu). \quad (13)$$

Then the small experimental value of ${}^{79}\delta\nu_s^{(2)} = 0.33$ MHz restricts the possible range of μ either near zero ($\mu \leq 0.017$, $\theta \geq 82^\circ$) or near one ($\mu \geq 0.983$, $\theta \leq 7.4^\circ$). If $\mu \simeq 1$ ($\theta \simeq 0$), ${}^{79}\nu_Q \simeq {}^{79}\delta\nu^{(1)} = 72.46$ MHz from Eqs. (6a) and (11). Then from Eq. (6b), ${}^{79}\delta\nu_c^{(2)} \simeq 2.506\eta^2$ (MHz).

Table III. Calculated Br NMR frequencies. The numbers in parentheses indicate the difference from the experimental values shown in Table I.

	ν_{sl} (MHz)	ν_c (MHz)	ν_{sh} (MHz)
^{79}Br	102.53 (0.09)	185.97 (-0.01)	247.38 (0.02)
^{81}Br	127.31 (-0.03)	195.64 (0.08)	249.85 (-0.05)

However, this is clearly incompatible with the experimental value of 11.41 MHz (Eq. 10). Therefore, possible solutions must satisfy $\mu \simeq 0$ ($\theta \simeq 90^\circ$).

The possible ranges of parameter values are determined as follows. We first fix the value of μ . Then $^{79}\nu_Q$ is expressed by η and α using Eq. (6a) and the experimental value of $^{79}\delta\nu^{(1)}$. By putting this expression into Eqs. (6b) and (6c), the values of η and α are determined by solving these equations using the experimental values of $^{79}\delta\nu_c^{(2)}$ and $^{79}\delta\nu_s^{(2)}$. We found that solutions exist only for $0 \leq \mu \leq 0.0024$ ($90^\circ \leq \theta \leq 87.2^\circ$). For this range of θ , other parameters take the values, $-0.85 \leq \alpha \leq -1$ ($74^\circ \leq \phi \leq 90^\circ$), $0.31 \geq \eta \geq 0.28$, and $114.7 \leq ^{79}\nu_Q \leq 115.1$ MHz. The magnitude of the internal field is obtained as $B_{\text{int}} = ^{79}\nu_0 / ^{79}\gamma = 16.37$ T. Thus the second order perturbation analysis significantly narrows down the possible range of the parameters.

We have further refined the parameter values obtained above by numerical diagonalization of the nuclear Hamiltonian to calculate χ^2 and by seeking the minimum of χ^2 . We have changed the value of each parameter successively within an appropriate range to find the global minimum of χ^2 by iteration. Then the final adjustment of the parameter values was done by using parabolic expansion of χ^2 with respect to the parameters to calculate the precise location of the minimum and to estimate uncertainties of the parameter values. The final results are the following:

$$\begin{aligned}
 B_{\text{int}} &= 16.40 \pm 0.01 \text{ (T)} \\
 ^{79}\nu_Q &= 112.5 \pm 0.4 \text{ (MHz)} \\
 \eta &= 0.330 \pm 0.005 \\
 \theta &= 89.5^\circ \pm 1.0^\circ \\
 \phi &= 87.8^\circ \pm 4.9^\circ,
 \end{aligned} \tag{14}$$

with $\chi^2 = 1.8$. The resonance frequencies calculated from these parameter values are compared with the experimental data in Table III. The finite value of η indicates lack of C_4 -symmetry at the Br sites, similarly to the Cl sites in $(\text{CuCl})\text{LaNb}_2\text{O}_7$ where $\eta = 0.56$,⁷⁾ again ruling out the tetragonal $P4/mmm$ space group.

4.2 Cu sites

Applying the same perturbation analysis to the Cu data, we obtain the following values of the Zeeman frequency, the first and the second order quadrupolar shifts for the ^{63}Cu nuclei, $^{63}\nu_0 = 64.2 \pm 2.0$ MHz ($B_{\text{int}} = 5.7$ T), $^{63}\delta\nu^{(1)} = 28.05 \pm 0.29$ MHz, $^{63}\delta\nu_c^{(2)} = 0.3 \pm 2.1$ MHz, $^{63}\delta\nu_s^{(2)} = 0.5 \pm 2.1$ MHz. The rather large uncertainties of these values, however, prevent us from narrowing the range of parameter values efficiently.

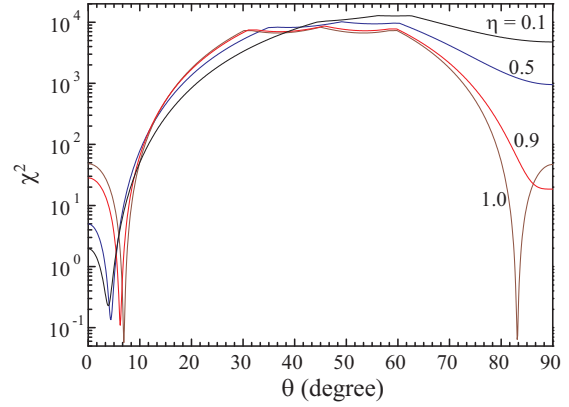


Fig. 4. (color online). The θ -dependence of χ^2 of the Cu NMR spectrum for various values of η . Values of other parameters are chosen to minimize χ^2 : $B_{\text{int}} = 5.716$ T, $^{63}\nu_Q = 28.31$ MHz, $\phi = 1.3^\circ$ for $\eta = 0.1$, $B_{\text{int}} = 5.705$ T, $^{63}\nu_Q = 28.45$ MHz, $\phi = 89.8^\circ$ for $\eta = 0.5$, $B_{\text{int}} = 5.680$ T, $^{63}\nu_Q = 29.03$ MHz, $\phi = 90^\circ$ for $\eta = 0.9$ and $B_{\text{int}} = 5.670$ T, $^{63}\nu_Q = 29.38$ MHz, $\phi = 88.7^\circ$ for $\eta = 1.0$. Note that χ^2 always takes one deep minimum at a small value of θ ($\theta \leq 6^\circ$) except when η is very close to one.

In fact, the experimental Cu resonance frequencies can be reproduced quite well by numerical diagonalization of the nuclear Hamiltonian for any value of η between 0 and 1 as shown in Fig. 4, where χ^2 is plotted against θ for several values of η with other parameter values fixed to minimize χ^2 . The χ^2 always shows a single deep minimum well below one at a small value of θ , $\theta \leq 7^\circ$, except when η is very close to one. For $\eta = 1$, there are two minima in χ^2 at $\theta = 6^\circ$ and at $\theta = 83^\circ$. The optimized values of B_{int} and $^{63}\nu_Q$ minimizing χ^2 depend only slightly on η : $B_{\text{int}} = 5.72$ T and $^{63}\nu_Q = 28.3$ MHz for $\eta = 0$ change to $B_{\text{int}} = 5.67$ T and $^{63}\nu_Q = 29.4$ MHz for $\eta = 1$. The optimized value of ϕ stays at 90° when $\eta \geq 0.3$. When η is small ($\eta \simeq 0.1$), ϕ cannot be determined since the Hamiltonian itself depends only weakly on ϕ .

Let us compare these results with those obtained for the non-magnetic $(\text{CuCl})\text{LaNb}_2\text{O}_7$ by Cu NMR experiments at various magnetic fields.⁷⁾ By assuming that the c -axis is one of the principal axes of the EFG, it was found that the z -axis with the largest principal value of EFG in $(\text{CuCl})\text{LaNb}_2\text{O}_7$ lie in the ab -plane, $^{63}\nu_Q = 29.64$ MHz and $\eta = 0.098$.⁷⁾ We notice that the values of $^{63}\nu_Q$ are almost identical for the two materials, indicating the similar local structure. We also expect that they have similar values of η . Therefore, it is very unlikely that η in $(\text{CuBr})\text{LaNb}_2\text{O}_7$ is close to one. Then we conclude from the above results that θ is very small ($\theta \leq 6^\circ$) in $(\text{CuBr})\text{LaNb}_2\text{O}_7$. The analysis of the Cu spectrum in $(\text{CuBr})\text{LaNb}_2\text{O}_7$ demonstrates that the Cu-NMR spectrum can be well reproduced by the EFG parameters which are nearly equal to those for $(\text{CuCl})\text{LaNb}_2\text{O}_7$ and the internal field of about 5.7 T must be directed nearly parallel to the z -axis of the EFG tensor, which corresponds to the largest principal value of EFG.

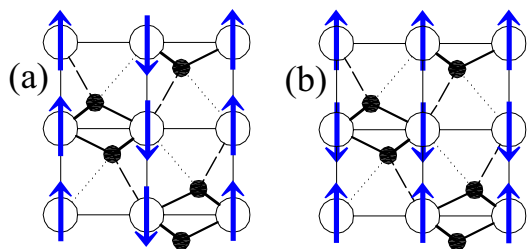


Fig. 5. (color online). Possible spin configurations of the collinear order on the distorted lattice. Only the pattern (b) is compatible with the large internal field observed at the Br sites.

5. Discussion

Summarizing the analysis in the previous sections, we found the following: (1) There is an internal field of 5.7 T at the Cu sites directed along the z -axis of the EFG. (2) There is an internal field of 16.4 T at the Br sites directed perpendicular to the z -axis of the EFG.

Let us first discuss the results on the Cu sites. Since the value of ν_Q at the Cu site is nearly the same for the Br and Cl compounds, we expect the two compound to have the same z -axis of the EFG, which was found to be in the ab -plane in $(\text{CuCl})\text{LaNb}_2\text{O}_7$.⁷⁾ The internal field directed along the z -axis in $(\text{CuBr})\text{LaNb}_2\text{O}_7$ is then consistent with the neutron results reporting the ordered moment parallel to the b -axis.⁴⁾ The internal field at the Cu nuclei is mainly due to the magnetic moment on the same Cu ion being observed (the on-site hyperfine field), which is anisotropic reflecting the anisotropic shape of the Cu-3d orbital. It is concluded from the anisotropy of the Cu NMR shift in $(\text{CuCl})\text{LaNb}_2\text{O}_7$ that the Cu spin is mainly on the $d(3y^2 - r^2)$ orbital, where y is parallel to the crystalline c -axis.⁷⁾ The internal field of 5.7 T then corresponds to the magnetic moment of $0.5 \pm 0.1 \mu_B$ in the ab -plane from the hyperfine coupling constant $A_{\perp}^{\text{hf}} = -11 \pm 2 \text{ T}/\mu_B$.⁷⁾ This value is consistent with the ordered moment of $0.6 \mu_B$ observed by neutron diffraction.⁴⁾

We next discuss the results on the Br sites. In contrast to the Cu sites, the internal field at the Br sites is due to the transferred hyperfine interaction, which is the coupling between the magnetic moments and the ligand nuclei through the covalency effects. If the structure were the tetragonal $P4/mmm$,¹⁾ the Br nuclei would couple equally to the four nearest neighbor Cu moments. Then the total internal field would have to be cancelled out to zero for the collinear AF order with the wave vector $(\pi, 0, \pi)$, which was observed by neutron diffraction experiments.⁴⁾ The finite internal field at the Br sites, therefore, gives direct evidence for structural distortion breaking the four-fold symmetry at the Br sites. The finite value of η , the asymmetry parameter of EFG, at the Br sites is another independent piece of evidence for such structural distortion. Yet, the sharp six peaks in the Br-NMR spectrum ensure a unique crystallographic site without appreciable disorder.

These features of the local symmetry at the Br sites are exactly what were found for the Cl sites in $(\text{CuCl})\text{LaNb}_2\text{O}_7$,⁷⁾ which have led Yoshida *et al.* to propose possible structural models with orthorhombic dis-

tortion shown in Fig. 2. We now examine if the same models provide consistent account for the results on $(\text{CuBr})\text{LaNb}_2\text{O}_7$ as well. In $(\text{CuCl})\text{LaNb}_2\text{O}_7$, the z -axis of the EFG at the Cl sites is parallel to the c -axis. This is likely to hold also for the Br sites in $(\text{CuBr})\text{LaNb}_2\text{O}_7$, since the internal field at the Br sites should be parallel to the Cu moments, which lie in the ab -plane, and $\theta = 90^\circ$. This prefers the model (a) rather than (b) and (c) shown in Fig. 2, since the Cl (or Br) sites are then on the mirror plane, therefore, the c -axis can be a principal axis. Yoshida *et al.* have argued that the displacement of Cl atoms makes the exchange coupling shown by the red lines in Fig. 2 much stronger than the other bonds, leading to local dimer singlet formation in $(\text{CuCl})\text{LaNb}_2\text{O}_7$.

If this bond remains strong and antiferromagnetic in $(\text{CuBr})\text{LaNb}_2\text{O}_7$, the collinear AF order shown in Fig. 5(a) should appear. In this structure, however, Br nuclei couple dominantly to two antiparallel moments, therefore, the internal field can never be as large as 16.4 T. In fact, the observed internal field is nearly equal to those reported for $(\text{CH}_3\text{NH}_3)_2\text{Cu}(\text{Cl}_{1-x}\text{Br}_x)_4$ (15.8 and 15.2 T),¹⁸⁾ which is a typical example of strong transferred hyperfine interaction via the σ -bond between Cu- $d(x^2 - y^2)$ orbital and the Br- p_σ orbital. The transferred hyperfine interaction should be weaker for a Br-Cu pair in $(\text{CuBr})\text{LaNb}_2\text{O}_7$, where the spin density is mainly on the $d(3y^2 - r^2)$ orbital. Thus the large internal field of 16.4 T is possible only if the hyperfine fields from two Cu spins add. In other words, the Br nuclei must couple dominantly to two parallel moments as shown in Fig. 5(b).

The same hybridization process involved in the transferred hyperfine interaction also causes the superexchange interactions. The strong asymmetry in the transferred hyperfine interaction, then induces inequivalent exchange interactions. The models shown in Fig. 2(a), for example, include five distinct exchange interactions. It is known that the superexchange interaction through the path Cu-X-Cu is very sensitive to small structural variation and often changes sign.¹⁹⁾ Therefore, it is conceivable that dominant exchange coupling changes from antiferromagnetic in $(\text{CuCl})\text{LaNb}_2\text{O}_7$ to ferromagnetic in $(\text{CuBr})\text{LaNb}_2\text{O}_7$ by small difference in the ionic position, even if the both compounds show the same type of structural distortion.

From the susceptibility and the magnetization data, however, it is unlikely that single ferromagnetic interaction dominate over other interactions in $(\text{CuBr})\text{LaNb}_2\text{O}_7$. The Weiss temperature θ_W , defined by the Curie-Weiss law of the susceptibility $\chi = C/(T + \theta_W)$, changes from 9.6 K in $(\text{CuCl})\text{LaNb}_2\text{O}_7$ ²⁾ to 5.1 K in $(\text{CuBr})\text{LaNb}_2\text{O}_7$.¹³⁾ The positive value of θ_W indicates that averaged interaction is still antiferromagnetic in $(\text{CuBr})\text{LaNb}_2\text{O}_7$, even though it is less so compared with $(\text{CuCl})\text{LaNb}_2\text{O}_7$. The saturation field B_c of the magnetization curve gives a measure of stability of the antiferromagnetic state. The increase of B_c from 30 T in $(\text{CuCl})\text{LaNb}_2\text{O}_7$ ³⁾ to 70 T in $(\text{CuBr})\text{LaNb}_2\text{O}_7$ ¹³⁾ points to higher stability of the antiferromagnetic state in $(\text{CuBr})\text{LaNb}_2\text{O}_7$, presumably due to overall increase of exchange interaction in Br compounds. It appears that the different ground states in the Cl and Br compounds

is the results of subtle balance among several inequivalent frustrating interactions. Precise theoretical studies are desired to relate our structural model to the magnetic ground state.

6. Summary

We have presented the Cu and Br NMR spectra in the collinear antiferromagnetic state in $(\text{CuBr})\text{LaNb}_2\text{O}_7$ at zero magnetic field and $T = 4.2$ K and determined the values of the internal field, EFG tensor and their relative orientation. The results at the Cu sites confirmed an AF order of about $0.5 \pm 0.1 \mu_B/\text{Cu}$ in the ab -plane. In order for the large internal field at the Br sites to be compatible with the collinear AF order observed by neutrons, the Br sites must be displaced from the center of the Cu square lattice to couple strongly to only two parallel Cu spins. Our results in $(\text{CuBr})\text{LaNb}_2\text{O}_7$ can be explained consistently by the structural model proposed for $(\text{CuCl})\text{LaNb}_2\text{O}_7$, provided that the pairs of Cu spins, which form singlet dimers in the Cl compound, are aligned parallel in the Br compounds due to modified exchange interactions brought by small difference in the ionic displacement.

Acknowledgment

This work was supported by Grant-in-Aid for Scientific Research (Nos. 18740202 and 17684018) and Grant-in-Aids on Priority Areas “Invention of Anomalous Quantum Materials” (Nos. 16076204 and 16076210) and “Novel State of Matter Induced by Frustration” (No. 19052004) from the MEXT Japan.

1) T. A. Kodenkandath, J. N. Lalena, W. L. Zhou, E. E. Carpenter, C. Sangregorio, A. U. Falster, W. B. Simmons, C. J. O'Connor, and J. B. Wiley: *J. Am. Chem. Soc.* **121** (1999) 10743.

2) H. Kageyama, T. Kitano, N. Oba, M. Nishi, S. Nagai, K. Hirota, L. Viciu, J. B. Wiley, J. Yasuda, Y. Baba, Y. Ajiro, and K. Yoshimura: *J. Phys. Soc. Jpn.* **74** (2005) 1702.
 3) H. Kageyama, J. Yasuda, T. Kitano, K. Totsuka, Y. Narumi, M. Hagiwara, K. Kindo, Y. Baba, N. Oba, Y. Ajiro, and K. Yoshimura: *J. Phys. Soc. Jpn.* **74** (2005) 3155.
 4) N. Oba, H. Kageyama, T. Kitano, J. Yasuda, Y. Baba, M. Nishi, K. Hirota, Y. Narumi, M. Hagiwara, K. Kindo, T. Saito, Y. Ajiro and K. Yoshimura: *J. Phys. Soc. Jpn.* **75** (2006) 113601.
 5) Y. Tsujimoto, Y. Baba, N. Oba, H. Kageyama, T. Fukui, Y. Narumi, K. Kindo, T. Saito, M. Takano, Y. Ajiro, and K. Yoshimura: *J. Phys. Soc. Jpn.* **76** (2007) 063711.
 6) A. Kitada, Z. Hiroi, Y. Tsujimoto, T. Kitano, H. Kageyama, Y. Ajiro, and K. Yoshimura: *J. Phys. Soc. Jpn.* **76** (2007) 093706.
 7) M. Yoshida, M. Ogata, M. Takigawa, J. Yamaura, M. Ichihara, T. Kitano, H. Kageyama, Y. Ajiro, and K. Yoshimura: *J. Phys. Soc. Jpn.* **76** (2007) 104703.
 8) T. A. Kodenkandath, A. S. Kumbhar, W. L. Zhou, J. B. Wiley, *Inorg. Chem.* **40** (2001) 710.
 9) G. Misguich and C. Lhuillier: in “Frustrated spin systems”, H. T. Diep Ed., (WorldScientific, Singapore 2003); *cond-mat/0310405*.
 10) N. Read and S. Sachdev: *Phys. Rev. Lett.* **62** (1989) 1694.
 11) N. Shannon, B. Schmidt, K. Penc, and P. Thalmeier: *Eur. Phys. J. B* **38** (2004) 599.
 12) G. Caruntu, T. A. Kodenkandath, and J. B. Wiley: *Mater. Res. Bull.* **37** (2002) 593.
 13) N. Oba, H. Kageyama, T. Saito, M. Azuma, W. Paulus, T. Katano, Y. Ajiro, and K. Yoshimura: *J. Mag. Mag. Mat.* **310** (2007) 1337.
 14) C. P. Slichter: “*Principles of Magnetic Resonance*” (Springer-Verlag Berlin Heidelberg, 1990).
 15) A. Abragam: “*The principles of Nuclear Magnetism*” (Oxford Univ. Press, New York, 1961).
 16) G. H. Stauss: *J. Chem. Phys.* **40** (1964) 1988.
 17) J. Bieron, P. Pyykkö, D. Sundholm, V. Kello, and A. J. Sadlej: *Phys. Rev. A* **64** (2001) 052507.
 18) H. Kubo, Y. Suzuki, and T. Akitomi: *J. Phys. Soc. Jpn.* **47** (1979) 2029.
 19) Y. Inagaki, A. Kobayashi, T. Asano, T. Sakon, H. Kitagawa, M. Motokawa and Y. Ajiro: *J. Phys. Soc. Jpn.* **74** (2005) 2683.